

# Analytical Model to Establish the Thermal Conductivity of Porous Structure

C. H. Mao<sup>a\*</sup>, M. A. Othuman Mydin<sup>b</sup>, X. B. Que<sup>c</sup>

<sup>a</sup>School of Civil Engineering, Harbin Institute of Technology, No. 11 Siling Street, Nangang District, 150001, Harbin, China

<sup>b</sup>School of Housing, Building and Planning, Universiti Sains Malaysia, 11800, Penang, Malaysia

<sup>c</sup>School of Civil Engineering and Architecture, Central South University, Changsha City, 410083, Hunan Province, China

\*Corresponding author: chmao65@gmail.com

## Article history

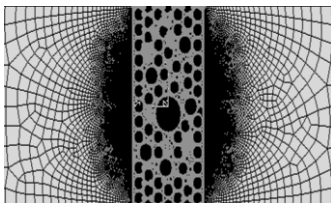
Received :20 January 2014

Received in revised form :

6 April 2014

Accepted :15 June 2014

## Graphical abstract



## Abstract

The presented research paper deals with analytical method to determine the thermal conductivity of porous material (intumescent coating) where the main objective is to assess whether it is possible to treat the voids in intumescent coating as having a uniform diameter. Considering the nature of intumescent coating, the mechanisms of its fire retardant properties are expansion and heat absorption. A predictive model should therefore include prediction of expansion behaviour, energy and mass conservation based on both physical and chemical behaviour, and also thermal conductivity of the coating. A 3-D analytical model will be developed to determine the thermal conductivity of intumescent coating. Finite Element simulations using ABAQUS also will be performed to assess the influence of different pore size distributions. The results of this numerical study indicate that, given the same porosity, the overall thermal conductivity of the porous structure is very close to that with uniform distribution of pores of the dominant size. This strongly suggests that, given the difficulty of obtaining precise pore size distribution, it is reasonable to treat an intumescent coating as having a uniform distribution of pores of the same size.

*Keywords:* Analytical model; porous material; coating; fire retardant; thermal properties

## Abstrak

Kertas kajian ini membentangkan kaedah analisis untuk menentukan keberaliran haba bahan berliang (salutan "intumescent" di mana objektif utama adalah untuk menilai sama ada bermungkinan untuk merawat lompong dalam salutan "intumescent" yang mempunyai diameter seragam. Memandangkan sifat salutan "intumescent", di mana mekanisme kalis api adalah pengembangan dan penyerapan haba. Oleh itu, model ramalan harus merangkumi ramalan tingkah laku pengembangan, tenaga dan pemuliharaan besar-besaran berdasarkan kedua-dua tingkah laku fizikal dan kimia, dan juga kekonduksian terma lapisan. Model analisis 3-D akan dibangunkan untuk menentukan kekonduksian haba salutan "intumescent". Simulasi FEM menggunakan ABAQUS juga akan dilakukan bagi menilai pengaruh taburan saiz liang yang berbeza. Keputusan kajian berangka ini menunjukkan bahawa, memandangkan ke-liang yang sama, kekonduksian terma keseluruhan struktur berliang sangat dekat dengan pengagihan seragam liang saiz yang dominan. Ini menunjukkan bahawa, memandangkan kesukaran mendapatkan tepat taburan saiz liang, adalah munasabah untuk merawat salutan "intumescent" sebagai mempunyai taburan seragam daripada liang-liang yang sama saiz.

*Kata kunci:* Model analitikal; bahan berliang; salutan; kalis api; properti terma

© 2014 Penerbit UTM Press. All rights reserved.

## 1.0 INTRODUCTION

Intumescent coating consists of reactive intumescent additives bound together by an organic resin binder. The binder has a number of functions to fulfill, particularly in controlling char expansion and ensuring a uniform foam structure [1]. From this point of view, the resin binder is a fundamental important point to study; many types of materials have been investigated and applied by research organizations and industries [2]. Polyurethane, Epoxy,

Polypropylene are most widely used according to different design guidance. Most of the published information on intumescent coatings is in the patent literature, whereas little is reported on the chemical-physical mechanism of intumescent. It can be generally classified that the reactive chemical compounds of intumescent systems include three categories: inorganic acid sources, carbon-rich polyhydric compound and organic amine or amide [3].

In intumescent systems, it is essential that the different components incorporated show a suitable matching thermal behavior: a random selection of a component of each of the three classes mentioned above does not ensure intumescent behaviour in their mixture. Careful design is required to ensure the intumescent system to provide effective fire protection. In fact, the order and timing of chemical and physical processes are critical, they must happen in an appropriate sequence [4].

Firstly, the inorganic acid source must be dehydrated to release acid. Secondly, the acid will dehydrate the carbon-rich polyhydric compound in preparation for the eventual formation of a solid char. Thirdly, the blowing agent evolves the gas, the gas then diffuses into small bubbles at nucleation sites, resulting in the formation of foam. Finally, the carbonaceous products from previous step then solidify through cross-linking into a multi-cellular char, simultaneously with the gas evolution. Of particular importance is the appropriate matching of rate of gas evolution and viscosity of charring compound, both of which depend on the temperature [3]. If gasification takes place when the polymer melt is too viscous, bubble growth will be strongly opposed, and the gas will tend to diffuse through the mixture without generating bubbles. If it happens when the polymer melt is too fluid, the bubbles will be large, resulting in a fragile and ineffective char [5].

## 2.0 INTUMESCENCE MECHANISMS

It is difficult to define the exact function of each component without detailed studies of chemical reactions which occur in the intumescence process. Furthermore, due to the multi-functional groups that exist within some compounds, these ingredients will perform more than one function [6]. The intumescence itself is a dynamic process, which makes the problem hard to be solved, so only some basic functions of the general additives mentioned previously in this chapter will be discussed. An inorganic acid source, which is usually the salt of an inorganic/non-volatile acid, is freely mixed with a polymer or formed in situ by a precursor, will undergo thermal decomposition normally at temperatures of 100°C–250°C, yielding an acid. The resulting acid will then trigger the solidification reaction later in the series [Camino, 1984]. The organic amine or amide, which is generally known as blowing agent, will decompose at temperatures of 300°C–350°C to release a large volume of gas responsible for the bubbling process. Compounds such as urea, melamine, and dicyandiamide of urea-formaldehyde resins are often introduced into intumescent formulations to act as blowing agents. In each case they should be carefully selected in order to have a suitable match between blowing and charring processes. Melamine is the name given to the molecule 2, 4, 6-triamino-s-triazine, which was first synthesized in 1834.

Carbon-rich polyhydric compounds can be dehydrated to form the backbone of the carbonaceous foam, where this dehydration is catalyzed by the acid produced from inorganic acid source. As the reaction keeps going, the polyol ester will melt and break into pieces. Carbon residue is left as rigid backbone structure. Ammonium polyphosphate (APP) and pentaerythritol (PER) system would be the most typical one in studies of intumescent mechanisms. It was first mentioned by Vandersall [7] in his review paper. He suggested that APP lost ammonia to form polyphosphoric acid, which then reacted with the PER alcohol groups to form a phosphate ester bond.

It should be pointed out that intumescent coating provides fire resistance to the protected structures by its expansion. The formation of a multi-cellular char leads to a significant reduced thermal conductivity, thereby contributing to the insulation

function of the material. The thermal conductivity of an intumescent coating is a key parameter to evaluate its fire protection performance. Therefore, correct calculation of its thermal conductivity is extremely important for accurate assessment of the fire protection performance of the coating system. When an intumescent coating expands at high temperatures, numerous bubbles are formed. It is clearly not possible for these bubbles to develop the same size and to be uniformly dispersed in the intumescent coating foam. Yet it will be impossible to track the size and distribution of the individual bubbles. Therefore, for simplicity, in the model used in this study, it is assumed that the bubbles are uniformly distributed within the foam and have the same diameters. In order to check that this assumption is reasonable, this paper will present the results of a numerical study to investigate the effects of non-uniform distribution of bubbles on the overall thermal conductivity of the foamed intumescent coating [8].

## 3.0 OVERALL THERMAL CONDUCTIVITY OF POROUS INTUMESCENT

Heat transfer through the expanded intumescent coating is considered as a combination of heat transfer through the solid phase and the gas phase (bubbles or pores). If the macroscopic scale is much larger than the randomly distributed individual pores and the pores are of the same size and uniformly distributed, it is possible to develop an analytical method to calculate the overall thermal conductivity of the coating. Previous work by Russell [9] has investigated similar cases (bricks with spherical voids, which were formed by bloating or by burning out the combustible particles), and has proposed an approximation on the basis that the pores are cubes, all of the same size and with solid walls of uniform thickness. Refer to Figure 1 which shows a representative unit cell used to characterize the geometry of this simplified case.

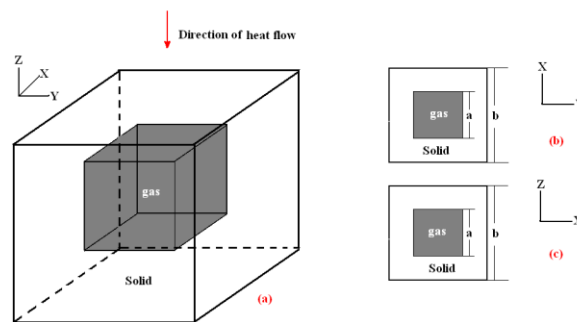


**Figure 1** Schematic of a unit cell for effective thermal conductivity calculation of a porous structure (a) 3-D view of the unit cell, (b) x-y view of the unit cell, (c) z-x view of the unit cell

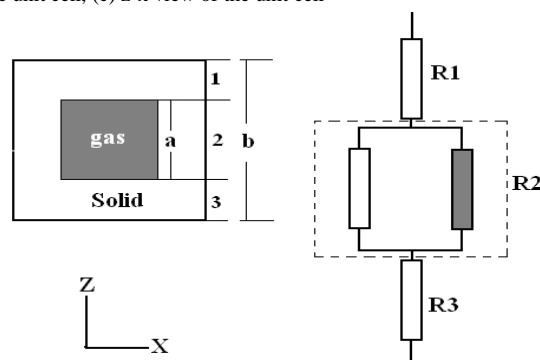


**Figure 2** Illustration of the 1-dimensional thermal resistance network along the direction of heat flow

Assume that the isothermal surfaces exist in planes, laws of conductors, in series and in parallel, can be used to express an idealized sketch of the one-dimensional model. Then the arrangement of the solid material and gas, integrated through the thickness of the coating, can be considered as a thermal resistance network, shown in Figure 2.

The equivalent thermal resistance  $R_{eq}$  of the unit cell can be estimated by summing the thermal resistance  $R_i$  in series:

$$R_{eq} = \sum_i R_i \quad (i=1,2,3) \quad (1)$$

Where the overall thermal resistance of the coating is defined by:

$$R_{eq} = \frac{b}{b^2 \lambda^*} \quad (2)$$

where  $\lambda^*$  is the overall thermal conductivity of the coating,  $b^2$  in the above equation is the planar area of the unit cell.

R1 and R3 represent the solid parts of the unit cell, therefore:

$$R_1 = R_3 = \frac{1}{2} \frac{(b-a)}{b^2 \lambda_s} \quad (3)$$

Where  $\lambda_s$  is the thermal conductivity of the solid.

For R2, it can be considered as a parallel resistance network, whose overall thermal resistance can be calculated as below:

$$R_2 = \frac{R_s R_g}{R_s + R_g} = \frac{\frac{a}{a^2 \lambda_g} \times \frac{a}{(b^2 - a^2) \lambda_s}}{\frac{a}{a^2 \lambda_g} + \frac{a}{(b^2 - a^2) \lambda_s}} \quad (4)$$

Where  $\lambda_g$  is the thermal conductivity of the gas.  $b^2$  in the above equation is the total planar area of the unit cell, and  $a^2$  in the equation represents the planar area occupied by the gas.

Substituting Equations 5.2, 5.3 and 5.4 into Equation 5.1, the overall thermal conductivity of the coating is obtained as:

$$\lambda^* = \lambda_s \frac{\lambda_g \varepsilon^{\frac{2}{3}} + (1 - \varepsilon^{\frac{2}{3}}) \lambda_s}{\lambda_g (\varepsilon^{\frac{2}{3}} - \varepsilon) + (1 - \varepsilon^{\frac{2}{3}} + \varepsilon) \lambda_s} \quad (5)$$

Where  $\varepsilon$  is the volume fraction (porosity) of the gaseous component ( $=a^3/b^3$ ).

Equation (5) will be used to calculate the overall thermal conductivity of the coating. For an expanded intumescent coating, the solid phase plays a minor part. It is important that the thermal conductivity of the gas inclusion (voids) is accurately calculated.

It should be pointed out that the simplification of using cubic inclusions is only considered when calculating the overall thermal conductivity of the foam, which is solely related to the volume fraction (porosity) of the porous structure. This assumption will be checked in Section 4.1. When dealing with the individual pores, the effective thermal conductivity is associated with a spherical shape as will be derived in section 3.1.2.

### 3.1 Thermal Conductivity of the Gas Inclusion

Heat transfer through the pores of a porous material should normally include all mechanisms of heat transfer: conduction, radiation and convection [10]. However, since the pores in an intumescent coating normally range from several hundred microns to less than 5 mm, natural convection within the pores is small and can be neglected [11]. In studies of porous materials, the radiative

component of heat transfer has often been neglected because these studies deal with heat transfer at ambient temperature or low temperatures. However, for fire applications where the temperatures are high, accurate calculation of heat transfer within the pores should also incorporate radiative heat transfer [9, 11]. Thus for this study, the equivalent thermal conductivity of the gas will consist of contributions from pure conduction (conductance through gas) and radiation.

#### 3.1.1 Conductance Through Gas

The available experimental data shows that the conductance related thermal conductivity of gas typically has strong temperature and pressure dependencies [Smith, 1998]. Under atmospheric pressure, the gas thermal conductivity was expressed as a function of temperature:

$$\lambda_{cond} = \lambda_{g0} \left( \frac{T}{T_0} \right)^{0.8} \quad (6)$$

Where  $\lambda_{g0}=0.0246\text{W/mK}$ , is thermal conductivity of gas at temperature  $T_0=273\text{K}$  ( $0^\circ\text{C}$ ).

A similar formulation has been given more recently by Di Blasi [12]. The thermal conductivity of gas, regardless its nature, is expressed as:

$$\lambda_{cond} = 4.815 \times 10^{-4} T^{0.717} \text{W} / \text{m} \cdot \text{K} \quad (7)$$

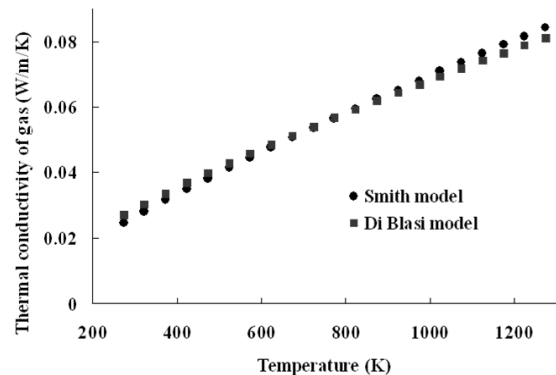


**Figure 3** Two different models of relationship between conductance related gas thermal conductivity and temperature

Figure 3 compares these two models of calculating conductance related thermal conductivity of gas. The results show that the two models produce very close values over a wide range of temperatures from 273K ( $0^\circ\text{C}$ ) to 1273K ( $1000^\circ\text{C}$ ). In this study, the Di Blasi's model has been selected for calculation.

#### 3.1.2 Radiation Through Gas

As temperature increases, thermal radiation becomes important and cannot be neglected in porous materials. The effect of thermal radiation across pores was discussed by Loeb [13], who has been accredited for the following equation to calculate the contribution of thermal radiation to the overall thermal conductivity of a pore:

$$\lambda_{rad} = 4Gde\sigma T^3 \quad (8)$$

Where  $G$  value is the average width of the pore divided by the maximum width of the pore and both quantities should be determined in the direction of the thermal gradient. Therefore,  $G$  is 1 for laminar pores and cylindrical pores with axes parallel to the heat flow direction,  $G$  is  $\pi/4$  for cylindrical pores with axes perpendicular to the heat flow direction. For spherical pores,  $G = 2/3$ .

Due to the difficulty in accessing the original article by Loeb [13], the following will present a derivation of Equation 5.8. Refer to Figure 4 which shows a spherical pore.

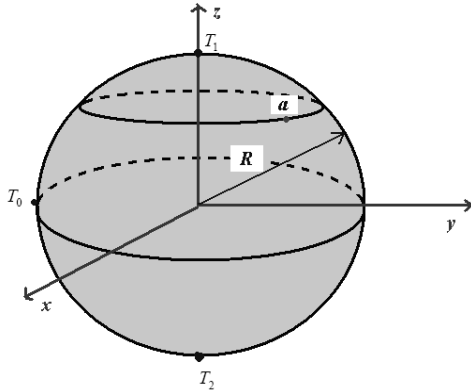


Figure 4 Illustration of a general spherical pore for calculation of radiation

For a surface element on the solid-pore boundary at  $a$ , the net value of normal component of radiation  $Q_a$  is equal to the difference between the heat flux leaving and the energy coming to the surface [14, 15]:

$$Q_a^r = e\sigma T_a^4 - e\sigma \int_A T_a^4 dF_{dA-dA'} \tag{9}$$

Where  $a'$  is any other emitting element on the surface of this spherical pore;  $A$  and  $A'$  represent allocated area for  $a$  and  $a'$ , respectively;

For a spherical enclosure it is obtained from simple geometric consideration as:

$$dF_{dA-dA'} = \frac{dA'}{4\pi R^2} \tag{10}$$

Thus, in this case, the second term on the right hand side of Equation 5.9 becomes constant:

$$Q_a^r = e\sigma \left( T_a^4 - \frac{1}{4\pi R^2} \int_A T_a^4 dA' \right) \tag{11}$$

From simple consideration, the mean temperature is:

$$T_0 = \frac{T_1 + T_2}{2} = \frac{1}{4\pi R^2} \int_A T_a dA' \tag{12}$$

Therefore the normal component of radiation becomes:

$$Q_a^r = e\sigma (T_a^4 - T_0^4) \tag{13}$$

Assuming  $T_a \approx T_0$ , then:

$$Q_a^r = 4e\sigma T_0^3 \Delta T \tag{14}$$

At the top point of this spherical pore, it has:

$$Q_1 = 4e\sigma T_0^3 (T_1 - T_0) \tag{15}$$

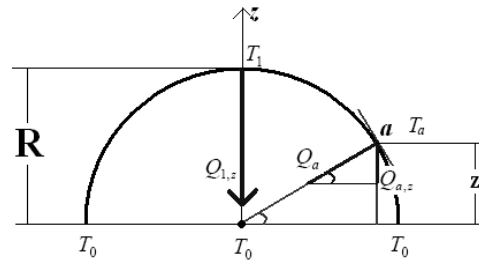


Figure 5 Calculation of radiation along heat flow direction

As demonstrated in Figure 5, heat flow is along the  $z$  axis, therefore only the  $z$  direction component of heat flux from every point “ $a$ ” is considered to make contribution to radiation through the whole pore. Because thermal gradient is linear along  $z$  direction, then:

$$T_a - T_0 = \frac{Z}{R} (T_1 - T_0) \Rightarrow Q_a = \frac{Z}{R} Q_1 \tag{16}$$

Where  $Z$  is coordinate of point  $a$  along  $z$  axis (central point of sphere is “0”)

The  $z$  component of radiation at point  $a$  is:

$$Q_{a,z} = \frac{Z}{R} Q_a \tag{17}$$

By simple calculation, the  $z$  direction component of heat flux from point “ $a$ ” is described as:

$$Q_{a,z} = Q_1 \times \frac{Z^2}{R^2} \tag{18}$$

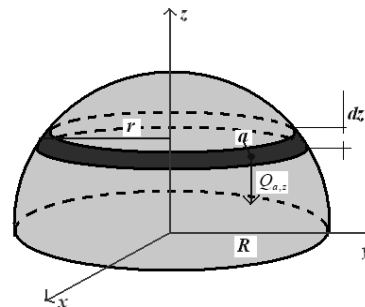


Figure 6 Calculation of total amount of radiation for a hemisphere

Refer to Figure 6, a ring strip is on the surface of hemisphere, with an infinitesimal height  $dZ$ . For a spherical surface, it can be proved that every ring strip that has the same height provides the same surface area. Therefore, for every single infinitesimal ring in Figure 6, the surface area can be expressed as:

$$S_{ring} = 2\pi R dZ \tag{19}$$

Heat responsible for  $z$  direction radiation is therefore calculated, for this ring surface:

$$H_z = Q_1 \frac{Z^2}{R^2} \times 2\pi R dZ \tag{20}$$

The total amount of  $z$  direction radiation of this hemisphere is obtained by integration:

$$H_{half} = \int_0^R Q_1 \frac{Z^2}{R^2} \times 2\pi R dZ = Q_1 \frac{2\pi}{R} \int_0^R Z^2 dZ = \frac{2\pi R^2}{3} Q_1 \quad (21)$$

In a simple way, the lower half of sphere provides the same effect as the upper half, so the total amount of heat transferred by radiation is:

$$H_{whole} = 2H_{half} = \frac{4\pi R^2}{3} Q_1 \quad (22)$$

The equivalent heat flux along the  $z$  direction over the projected area is:

$$Q_{eq} = \frac{H_{whole}}{\pi R^2} = \frac{4}{3} Q_1 \Rightarrow Q_{eq} = \frac{4}{3} \times 4e\sigma T_0^3 (T_1 - T_0) \quad (23)$$

Therefore, the effective thermal conductivity for radiation, within a sphere, is described as:

$$\lambda_{rad} = \frac{2}{3} \times 4de\sigma T^3 \quad (24)$$

### 3.1.3 Effective Thermal Conductivity of Gas

Combining the contributions to heat transfer in a pore by pure conduction and radiation, the total thermal conductivity of the gas within the pore can be given as:

$$\lambda_g = 4.815 \times 10^{-4} T^{0.717} + \frac{2}{3} \times 4de\sigma T^3 \quad (25)$$

## 4.0 INFLUENCES OF BUBBLE SIZE AND DISTRIBUTION

To check the influence of bubble size and distribution on thermal conductivity of intumescent coating, the commercial finite element analysis (FEA) software ABAQUS was used. This study was carried out in two steps: (1) to check the feasibility of using 2-D ABAQUS model to represent the 3-D coating because a 2-D ABAQUS model would take much less computational time to run; an auxiliary objective of this step is also to check whether Equation 5.5, which was derived on the basis of cubic inclusions, can be used more generally; (2) to use the verified 2-D model to investigate the effects of different bubble sizes and distributions.

### 4.1 Feasibility of using 2-D ABAQUS Model

For this check, the results of 2-D ABAQUS models will be compared with analytical results from Equation 5, which was developed on a 3-D basis assuming cubic pores. Two 2-D ABAQUS models are shown in Figure 7, one for circular inclusions and one for square inclusions. The models were constructed to have fixed applied temperatures at the top and bottom boundaries. If the temperatures at the top and bottom surfaces of a porous structure are fixed, the heat flux through the porous structure will not be uniform, which would introduce large errors in the results of thermal conductivity. To overcome this problem, two thick pieces of homogeneous material were introduced at the top and bottom surfaces of the studied porous layer, appearing in grey colour in Figure 7. While the porous part was 20 mm in thickness, each of the homogeneous attachments was assigned a 40 mm thickness. With this model, it is possible to achieve uniform heat flux and temperature at both the top and bottom surfaces.

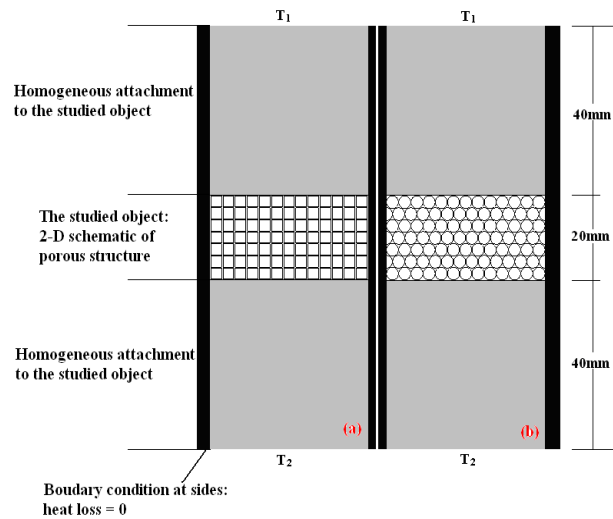


**Figure 7** 2-D ABAQUS simulation models (a) porous structure with square inclusions, (b) porous structure with circular inclusions

The overall thermal conductivity of this combined system can be obtained using Equation 26:

$$\lambda_{all} = Q \frac{\Delta T}{\Delta x_{all}} \quad (26)$$

Where  $Q$  is the heat flux observed at the surfaces (ABAQUS results),  $\Delta T$  is the temperature difference between top and bottom surfaces (input value), and  $\Delta x_{all}$  is the total thickness of the combined system (100mm).

The model shown in Figure 7 can be considered as an “in series” thermal conductor system. Hence, the thermal conductivity of the porous part can be calculated as:

$$\lambda_p = \frac{\lambda_{all} \lambda_h \varepsilon_p}{\lambda_h - \lambda_{all} (1 - \varepsilon_p)} \quad (27)$$

Where subscripts “ $p$ ”, “ $h$ ”, and “ $all$ ” denote the porous part, the homogeneous part, and the whole system, respectively, and  $\varepsilon_p$  represents the volume fraction of the porous part to the total volume. In this study, the thermal conductivity of the attachment material was given a value of 0.5W/m/K. The solid part of the porous structure was also assigned a thermal conductivity value of 0.5W/m/K. The pore inclusion of the porous structure was assigned a thermal conductivity value of 0.02W/m/K, which approximately represents the thermal conductivity of the gas at room temperature. The input temperature difference between the top and bottom surfaces was 0.2K.

The 2-D simulations were performed with different volume fractions of pores within the middle porous layer in Figure 7. The 2-D simulation results are compared with the 3-D analytical results (Equation 5.5) in Figure 8. It should be mentioned that in Figure 8, the volume fraction of pores (porosity) refers to that of the studied porous area, not the total area of the entire model. Good agreements can be seen between the 2-D simulation and the 3-D analytical model for both types of pore shape as well as different porosity, which confirms that, given the pore thermal conductivity, the overall thermal conductivity of a porous structure is mainly dependent on the porosity, with the pore shape having little effect.

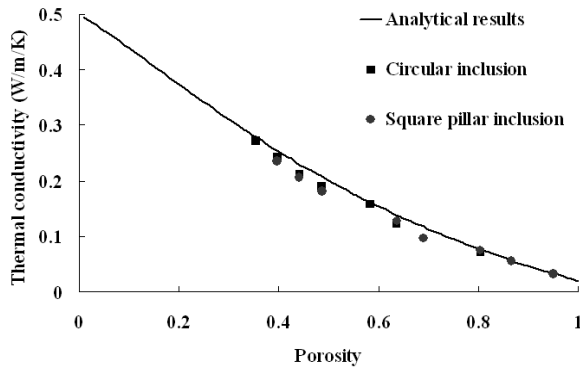


**Figure 8** Comparisons between the 2-D simulation results and the analytical model using Equation 5

**4.2 Various Bubble Size Effect at Different Temperatures**

To assess the influence of bubble size distribution, a number of numerical simulations were carried out using the ABAQUS 2-D model as described in the previous section. In this study, pores of different diameters were present in the models. To represent observations from the experiments, the majority of the pores were given diameter of 3 mm. Four other values of pore diameter were also included in the model, ranging from 0.5 mm to 7.937 mm (this specific value was used to keep the overall porosity constant). The total porosity was kept constant at 80.36%, in these different models, but the volume fractions of the different pore diameters were changed in each model. Table 1 list the different cases of the study. Case 1 represents a coating with uniform distribution of 3mm diameter pores. Case 2 represents a relatively equal fraction of the other four pore sizes. Cases 3 to 6 represent a significant volume of pores of one diameter while the volumes of the other three pore diameters were about equal but at much lower values.

**Table 1** Relative volume fractions of pores with different sizes for different study cases

Bubble diameter/ Relative volume fraction	3mm (%)	0.5mm (%)	1.139mm (%)	4mm (%)	7.937mm (%)
Case 1	100.00	0.00	0.00	0.00	0.00
Case 2	68.50	6.14	7.80	9.82	7.73
Case 3	65.20	4.79	6.69	7.86	15.47
Case 4	65.19	4.67	6.69	15.72	7.73
Case 5	65.19	4.67	12.58	9.82	7.73
Case 6	65.19	10.56	6.69	9.82	7.73

**Table 2** Numbers of pores of different diameters in different cases

Bubble diameter/ Number of bubbles	3mm	0.5mm	1.139mm	4mm	7.937mm
Case 1	91	0	0	0	0
Case 2	62	200	49	5	1
Case 3	59	156	42	4	2
Case 4	59	152	42	8	1
Case 5	59	152	79	5	1
Case 6	59	344	42	5	1

The different volume fractions were obtained as a result of fixing different numbers of pores of different diameters. Case 1 is the reference case, which has 91 circular inclusions of 3 mm in diameter in the 40 mm × 20 mm studied area, giving a porosity of 80.36%. In the other cases, the number of the 3 mm diameter bubbles was reduced while pores of the other four diameters were introduced into the studied area to represent non-uniform distribution of pores in more realistic situations. In all cases, the volume fraction of the 3mm pores is at about 65% of the total pore area. Table 2 lists the numbers of pores of different diameters used in the different cases.

Figure 9 shows a typical ABAQUS mesh, with a highly refined mesh in and around the porous structure. In all cases, 8-node heat transfer quadrilateral shell element DC2D8 was used. The element size was about 4mm near the top and bottom surfaces. In Case 1, the element size in and around the porous area was about 0.4mm, requiring about 15,000 elements in total. In other cases, due to non-uniform pore size distribution, a much finer mesh was used with the element size being about 0.1mm in and around the porous area. This increased the number of elements to around 140,000. Figures 10-15 show the enlarged porous area, indicating how pores of the different diameters were located in the different models.

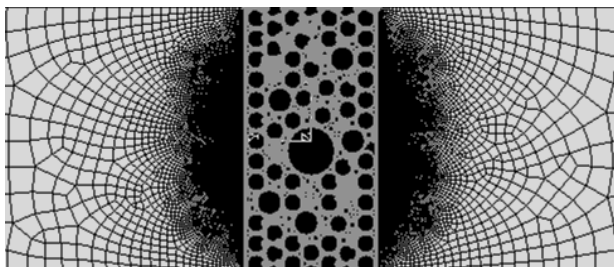


**Figure 9** A typical ABAQUS mesh

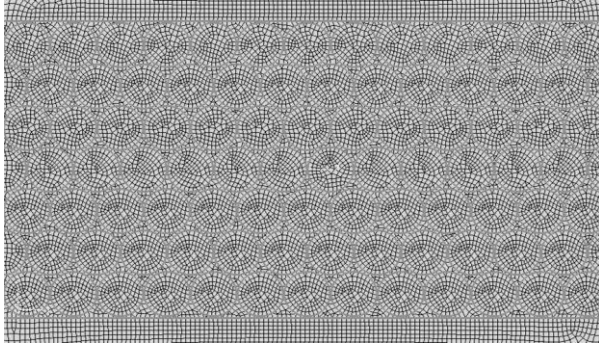


**Figure 10** Pore distribution in Case 1

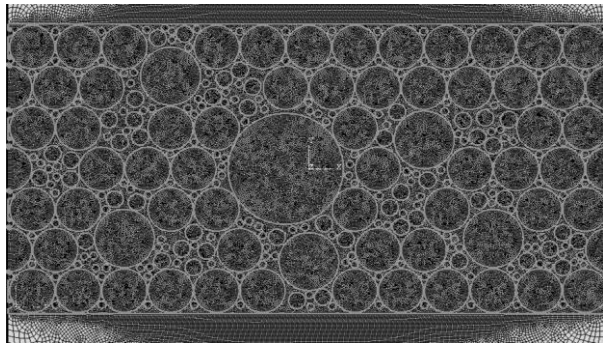


**Figure 11** Pore distribution in Case 2

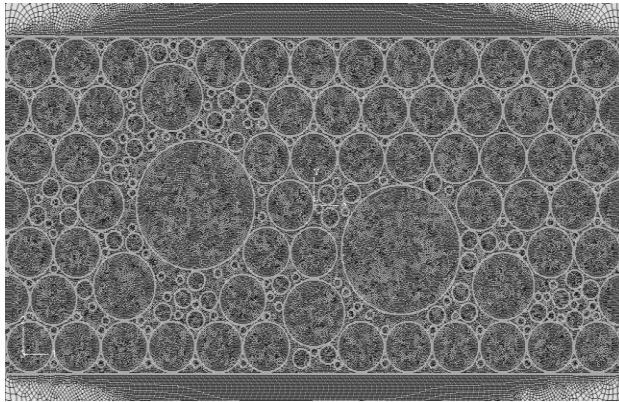


**Figure 12** Pore distribution in Case 3

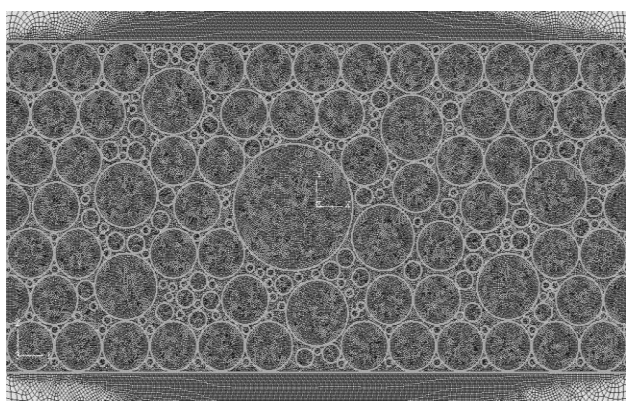


**Figure 13** Pore distribution in Case 4

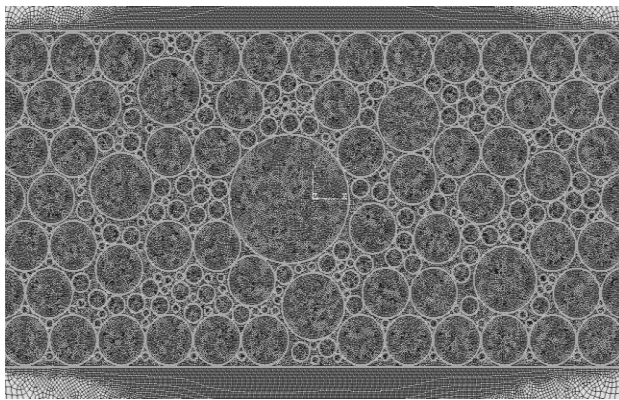


**Figure 14** Pore distribution in Case 5

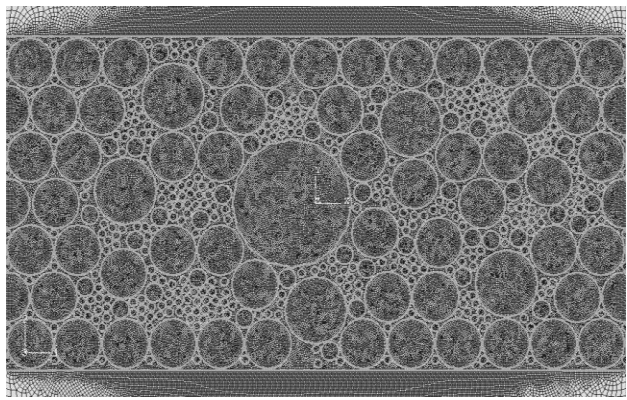


**Figure 15** Pore distribution in Case 6

ABAQUS simulations were performed to evaluate the effect on thermal conductivity of different pore size distributions at a range of temperatures. In these simulations, the solid matrix of the porous structure was assumed to have a constant thermal conductivity value, while the thermal conductivity of gas inclusions was calculated according to Equation 25 derived earlier in this chapter, considering both conductive and radiative contributions to the overall gas thermal conductivity. Therefore, the pore size is represented by its influence on gas thermal conductivity.

The different ABAQUS simulation Cases investigated the effect of different pore size distributions. Table 3-7 present the results of thermal conductivities at different temperatures for

pores of different diameters. Clearly, the radiative component becomes much greater than the conductive component at high temperatures. The overall thermal conductivity values of pores of the different sizes were used as input value in the ABAQUS simulations.

**Table 3** Thermal conductivity of 3mm pore at different temperatures

Temperature (K)	Conduction conductivity (W/m/K)	Radiation conductivity (W/m/K)	Thermal conductivity (W/m/K)
273	0.026874	0.008306	0.03518
373	0.033613	0.021186	0.054799
473	0.039854	0.043202	0.083055
573	0.045729	0.076803	0.122532
673	0.05132	0.12444	0.17576
773	0.056679	0.188562	0.245241
873	0.061845	0.271618	0.333463
973	0.066846	0.376057	0.442903
1073	0.071703	0.50433	0.576033
1173	0.076433	0.658885	0.735318
1273	0.081051	0.842172	0.923223

**Table 4** Thermal conductivity of 7.937 mm pore at different temperatures

Temperature (K)	Conduction conductivity (W/m/K)	Radiation conductivity (W/m/K)	Thermal conductivity (W/m/K)
273	0.026874	0.021975	0.048849
373	0.033613	0.05605	0.089664
473	0.039854	0.114297	0.154151
573	0.045729	0.203196	0.248925
673	0.05132	0.329227	0.380547
773	0.056679	0.498872	0.555551
873	0.061845	0.71861	0.780455
973	0.066846	0.994922	1.061768
1073	0.071703	1.334289	1.405992
1173	0.076433	1.74319	1.819623
1273	0.081051	2.228106	2.309157

**Table 5** Thermal conductivity of 4 mm pore at different temperatures

Temperature (K)	Conduction conductivity (W/m/K)	Radiation conductivity (W/m/K)	Thermal conductivity (W/m/K)
273	0.026874	0.011075	0.037949
373	0.033613	0.028248	0.061861
473	0.039854	0.057602	0.097456
573	0.045729	0.102404	0.148133
673	0.05132	0.16592	0.21724
773	0.056679	0.251416	0.308095
873	0.061845	0.362157	0.424002
973	0.066846	0.50141	0.568255
1073	0.071703	0.67244	0.744143
1173	0.076433	0.878513	0.954947
1273	0.081051	1.122896	1.203947

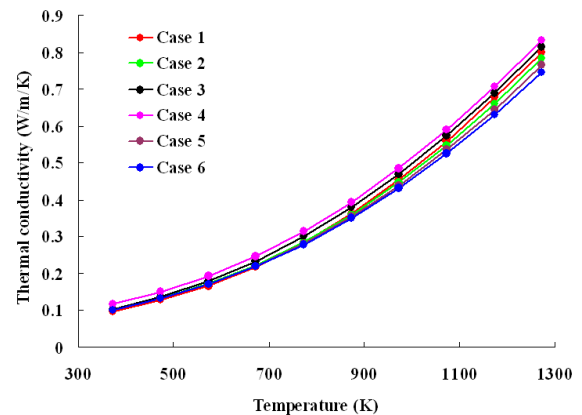
**Table 6** Thermal conductivity of 1.139 mm pore at different temperatures

Temperature (K)	Conduction conductivity (W/m/K)	Radiation conductivity (W/m/K)	Thermal conductivity (W/m/K)
273	0.026874	0.003154	0.030027
373	0.033613	0.008043	0.041657
473	0.039854	0.016402	0.056256
573	0.045729	0.02916	0.074889
673	0.05132	0.047246	0.098565
773	0.056679	0.071591	0.12827
873	0.061845	0.103124	0.164969
973	0.066846	0.142776	0.209622
1073	0.071703	0.191477	0.26318
1173	0.076433	0.250157	0.32659
1273	0.081051	0.319745	0.400796

**Table 7** Thermal conductivity of 0.5mm pore at different temperatures

Temperature (K)	Conduction conductivity (W/m/K)	Radiation conductivity (W/m/K)	Thermal conductivity (W/m/K)
273	0.026874	0.001384	0.028258
373	0.033613	0.003531	0.037144
473	0.039854	0.0072	0.047054
573	0.045729	0.012801	0.05853
673	0.05132	0.02074	0.07206
773	0.056679	0.031427	0.088106
873	0.061845	0.04527	0.107114
973	0.066846	0.062676	0.129522
1073	0.071703	0.084055	0.155758
1173	0.076433	0.109814	0.186248
1273	0.081051	0.140362	0.221413

In the subsequent ABAQUS simulations, the temperature difference between the top and bottom surfaces was kept at 0.2 K in every individual studies. Again, the solid part of the entire model, including the porous area, was assigned a thermal conductivity value of 0.5W/m/K. Table 8 presents the overall thermal conductivity of the porous area, calculated using Equation 27. These results are also plotted in Figure 16. Compared to the overall thermal conductivity of the reference case (Case 1), the maximum deviations at 1273K for the other cases are within a small range between 2%-7%.

**Figure 16** Comparison of the calculated overall thermal conductivity of the porous area in different cases

## 5.0 CONCLUSIONS

This paper has presented a 3-D analytical model for calculating the thermal conductivity of a porous structure. Derivations are also presented for calculating the total thermal conductivity of a spherical pore. Given the thermal conductivities of the solid and the gas components, the overall thermal conductivity is dependent solely on the volume fraction (porosity) of the gas component, with the shape of the pores which constitute the gas component having little effect.

Finite Element simulations using ABAQUS were performed to assess the influence of different pore size distributions. The results of this numerical study indicate that, given the same porosity, the overall thermal conductivity of the porous structure is very close to that with uniform distribution of pores of the dominant size. This strongly suggests that, given the difficulty of obtaining precise pore size distribution, it is reasonable to treat an

intumescent coating as having a uniform distribution of pores of the same size.

## References

- [1] Duquesnea, S., Magnet, S., Jama, C., Delobel, R. 2005. Thermoplastic Resins For Thin Film Intumescent Coatings E Towards A Better Understanding Of Their Effect On Intumescence Efficiency. *Polymer Degradation and Stability*. 88: 63–69.
- [2] Duquesnea, S., Magnet, S., Jama, C., Delobel, R. 2004. Intumescent Paints: Fire Protective Coatings for Metallic Substrates. *Surface and Coatings Technology*. 180: 302–307.
- [3] Camino, G., Costa, L., Martinasso, G. 1989. Intumescent Fire-Retardant Systems. *Polymer Degradation and Stability*. 23: 359–376.
- [4] Camino, G. 1993. *Fire Retardant Polymeric Materials, in Atmospheric oxidation and antioxidants*. Vol. II, Eds. G. Scott, Elsevier Amsterdam, Chap. 10.
- [5] Butler, K., Baum, H. R., Kashiwagi, T. 1997. *Three-Dimensional Modelling Of Intumescent Behaviour In Fires*. Fire Safety Science, Proc. 5th Int. Symp. 523.
- [6] Taylor, A. P. 1992. *The Materials Science of Intumescent Coatings*. Phd Thesis.
- [7] Vandersall, H. L. 1971. Intumescent Coating Systems, Their Development and Chemistry. *J. Fire and Flammability*. 2: 97–140.
- [8] Le Bras, M., Camino, G., Bourbigot, S., Delobel, R. 1998. (Eds.) *Fire Retardancy of Polymers the Use of Intumescence*. The Royal Society of Chemistry. Special Publication 224.
- [9] Russell, H. W. 1935. Principles of Heat Flow in Porous Insulators. *Journal of American Ceramic Society*. 18: 1–12.
- [10] Horn Jr, W. E. 2000. *Inorganic Hydroxides and Hydroxycarbonates: Their Function and Use as Flame-Retardant Additives*. In *Fire Retardancy of Polymeric Materials*, Ed. A. F. Grand and C. A. Wilkie, Marcel Dekker, New York. 285.
- [11] Yu, F. 2006. Gaosheng Wei, Xinxin Zhang, and Kui Chen, Two Effective Thermal Conductivity Models for Porous Media with Hollow Spherical Agglomerates. *International Journal of Thermophysics*. 27: 293–303.
- [12] Di Blasi, C., Branca, C. 2001. Mathematical Model for the Non steady Decomposition of Intumescent Coatings. *American Institute of Chemical Engineers Journal*. 47: 2359–2370.
- [13] Loeb, A. L. 1954. A Theory of Thermal Conductivity Of Porous Materials. *Journal of American Ceramic Society*. 37: 96–102.
- [14] Le Bras, M., Camino, G., Bourbigot, S., Delobel, R. 1998. (Eds.) *Fire Retardancy of Polymers the Use of Intumescence*. The Royal Society of Chemistry, Special Publication 224.
- [15] Camino, G., Lomakin, S. 2001. *Intumescent Materials, in Fire Retardant Materials*. Ed. A. R. Horrocks and D. Price, Woodhead Publishing and CRC Press Cambridge. 318.